ARTÍCULO ORIGINAL/*ORIGINAL ARTICLE*
http://dx.doi.org/10.14482/sun.34.1.9736

Effect of temperature in bursting of thalamic reticular cells

Efecto de la temperature en las descargas en ráfaga de la células del núcleo reticular del tálamo

Oscar E Hernández[1], Eduardo E Zurek[2], David Vera[3], Alfonso Cepeda-Emiliani[4]

Abstract

Objective: *To show the relation between the four parameters associated to bursting discharges of the thalamic reticular cells (TRNn): the maximum firing frequency (f_{max}) and the temperature at which it occurs (T_{fmax}), the range of temperatures defined as the full width at half maximum (ΔT_h) and the maximum specific low threshold calcium conductance (G_T).*
Materials and Methods: *In order to simulate the TRNn bursting activity, a computational simulation model was implemented using the NEURON software, which incorporates morphological and electrophysiological data, and stimuli properties closely related to reality.*
Results: *It was found that there are nonlinear relations between the parameters. The f_{max} frequency follows a quadratic growth with temperature and tends asymptotically towards a limit value with the maximum calcium conductance. In the same manner, ΔTh increases until reaching a limit value as function of f_{max} and G_T. However, the increment per frequency unit is bigger than the increment per conductance unit.*
Conclusions: *Four equations were obtained that model the relations between the parameters associated to bursting discharges of the TRNn in rats and other neurons with similar characteristics in different animal species.*

Keywords: TRN neuron; Computational simulation; Firing frequency; Temperature; Burst firing

Resumen

Objetivo: *Mostrar la relación entre los cuatro parámetros asociados a las descargas en ráfaga de las neuronas del núcleo reticular del tálamo (TRNn): la frecuencia máxima de descarga (f_{max}) y la temperatura a la cual se produce (T_{fmax}), el rango de temperaturas definido como ancho a media altura (ΔT_h) y la conductancia máxima de calcio de bajo umbral (G_T).*

Fecha de recepción: 15 de julio de 2017
Fecha de aceptación: 30 de agosto de 2017

[1] Departamento de Química y Biología, Universidad del Norte, km 5 vía a Puerto Colombia, Barranquilla, Colombia. Orcid: 0000-0003-4476-0055
[2] Departamento de ingeniería de sistemas, Universidad del Norte, km 5 vía a Puerto Colombia, Barranquilla, Colombia. Orcid: 0000-0002-9816-6863
[3] Departamento de Ciencias Naturales y exactas, Universidad de la Costa, Calle 58 N° 55-66, Barranquilla, Colombia. Orcid: 0000-0003-3955-5452
[4] Departamento de Medicina, Universidad del Norte, km 5 vía a Puerto Colombia, Barranquilla, Colombia. Orcid: 0000-0002-5269-7810
Correspondencia: Oscar Emilio Hernández Bustos, universidad del norte, km 5 vía puerto Colombia. Barranquilla, Colombia. Tel. +5753509509 ext 4284 ohernandezb@uninorte.edu.co

Salud uninorte
Vol. 34, N° 1, 2018
ISSN 0120-5552
eISSN 2011-7531

Materiales y métodos: *Para simular las descargas en ráfaga de las TRNn se implementó un modelo de simulación computacional usando el software NEURON, que incorpora datos morfológicos, electrofisiologicos y las propiedades de los estímulos en estrecha relación con la realidad.*

Resultados: *Se encontraron relaciones no lineales entre los parámetros. La frecuencia f_{max} crece de forma cuadrática con la temperatura y tiende asintóticamente a un valor límite con la conductancia. Así mismo, ΔT_h también se incrementan hasta alcanzar un valor límite en función de f_{max} y G_T. No obstante, es mayor el incremento por cada unidad de frecuencia que por cada unidad de conductancia.*

Conclusiones: *Se obtuvieron cuatro ecuaciones que modelan las relaciones entre los parámetros asociados a las descargas en ráfaga de las neuronas TRN en ratas y otras neuronas con características similares en diferentes especies animales.*

Palabras clave: Neurona del TRN; Simulación computacional; Frecuencia de disparo; Temperatura; Descarga en ráfaga

INTRODUCTION

Thalamic reticular nucleus neurons (TRNn) respond to inputs in two different activity modes called burst and tonic firing [1, 2, 3, 4]. Burst mode is caused by dendritic activation of low threshold calcium currents (I_T) during inhibitory inputs, and this is mediated by T-type calcium channels with the properties: low unitary conductance, fast inactivation, slow activation kinetics, negative steady-state inactivation at resting potential and resistant to dihydropyridme (DHP) [5, 6]. The tonic mode is generated in response to excitatory inputs. Current I_T is mediated by a specific low threshold calcium conductance (T-type conductance) and is expressed in various cells, tissues and organs of species with different ranges of internal temperature (ΔT) and maximum values of T-type conductance (G_T). These include nervous tissue, smooth muscle, endocrine glands, sperm, kidneys, and heart [7, 8, 9]. In the lateral geniculate nucleus of the cat, for example, G_T = (8,4 +/- 0,9) nS/cm^2 and ΔT = (36,9 – 38,0)°C [10]; in the thalamic ventrobasal nucleus of the rat, G_T = (37600 – 38600) nS/cm^2 and ΔT = (34,0 – 36,0)°C [11]; in the dorsal root ganglion of the chick, G_T = (0.020-0.025) nS/cm^2 and ΔT = (40,8 – 41,6)°C[12]; in the dorsal root ganglion of the mouse, G_T = 0,0072 nS/cm^2 and 0,0057 nS/cm^2, and ΔT = (36,5 – 38,0)°C[13]; and in human embryonic kidney 293 cells (HEK 293), G_T = 0.009 nS and ΔT = (36,0 – 37,5)°C[14].

Employing computational simulations, it was previously shown that bursts and tonic firings observed in a thalamic reticular nucleus (TRN) soma could be explained as a product of random synaptic inputs on distal dendrites [15]. Tonic firings are generated by random excitatory stimuli, while two different types of stimuli generate burst firings: inhibitory random stimuli and a combination of inhibitory (from TRNn) and excitatory (from corticothalamic and thalamocortical neurons) random stimuli. Other studies have highlighted the importance of burst discharge parameters such as number and patterning of spikes, firing frequency, and rhythm of firing in transport and neuronal information processing [16, 17, 18, 19, 20, 21, 22]. The burst activity mode has an important effect on information processing in thalamocortical circuits during different physiological states, such as synchronized sleep and anesthesia [23, 24].

Commonly, intracellular recordings of electrical activity are conducted at room temperature and not at physiological temperature [25, 26, 27, 28, 29]. Increases in the opening and closing rates of ion channels when temperature (T) rises 10°C above room temperature are expressed by the factor Q10, which is proportional to the activation energy [30, 31, 32, 33]. However, it has been found that the effects of temperature on T-type Ca^{+2} channels are nonlinear [34, 35]. Computational simulation offers multiple alternatives, not only for modifying electrical neuronal conduction properties, but also environmental conditions such as temperature [36, 37, 38, 39, 40]. Accordingly, employing computational simulations, this study shows a nonlinear relation between the maximum burst firing frequency (f_{max}) observed in TRNn and the temperature at which it is produced on the one hand, and G_T, on the other. For a given G_T, the range of temperatures at which TRNn responds in burst mode also increases nonlinearly (exponential growth), both with its f_{max} and its G_T conductance.

MATERIALS AND METHODS

In order to develop a realistic simulation, the use of a morphology (neuronal geometry) obtained from a neuronal reconstruction with real dimensions was considered, the application of stimulus that takes into account the randomness of the amplitudes and durations of both inhibitory and excitatory stimuli originating in other TRNn and in collaterals of thalamocortical and corticothalamic neurons, respectively; and the biophysics that are incorporated by the model allow for reproducing different types of neuronal responses and their properties.

Then, the activity of TRNn was simulated using a computational tool, developed in NEURON simulation environment [41, 42], that incorporated morphological and electrophysiological data, and the stimuli properties. The following parts of this section describe in detail each one of these aspects and the methodology for analyzing burst responses of TRNn.

MORPHOLOGICAL DATA

The geometrical data (Table 1) were obtained from a neuronal reconstruction of an intact TRN cell with 80 compartments (figure 1A), from the ventrobasal region of a rat [43]. The data files were downloaded from the web page of the SenseLab Project [44].

ELECTROPHYSIOLOGICAL MODEL

The biophysical model with high distal density of g_T (Table 2) corresponds to a TRN cell from the ventrobasal region of a rat and it was obtained from [43]. The data files were downloaded from reference the web page of the SenseLab Project [44]. Tables 3-6 include a summary of the main formulas used in reference [44] to develop the algorithms that model the biophysics of neurons TRNn.

STIMULI PROPERTIES

The typical bursts in the soma of the TRNn can be generated by joint trains of inhibitory and excitatory random stimuli in the distal dendrites [15]. TRNns are continuously bombarded by excitatory stimuli from the collaterals of thalamocortical and corticothalamic neurons [45, 46], and by inhibitory stimuli of other TRNn [47]. A dendrite can be stimulated by one or more inhibitory postsynaptic potentials (IPSP) and excitatory postsynaptic potentials (EPSP) resulting in a temporal and spatial summation into the same dendrite [48, 49]. Thus, each dendrite can contribute with a depolarizing or hyper-

polarizing potential directed toward the soma. The amplitude of this potential depends on the number of EPSPs and IPSPs that stimulate the dendrite, and in consequence, can be considered as a random event.

Then, the characteristics of all trains of stimuli were randomized following a uniform distribution and were estimated from the analysis of the results presented in references [47, 15]. The amplitude of each stimulus (square pulses) was in the range [-0.25, 0.1043] nA, the duration of each stimulus was in the range [0, 1.0507] ms and the start time varied within [80, 120] ms. 25 pulses were applied with delays in the range from 0 to 12.4000 ms, obtaining a frequency of 0.1553 kHz.

The simulation presented in this paper evaluates 60 distal dendrites, and a different train of random stimuli was applied to each one of them. The trains of stimuli have the same statistical properties, but each train has a different random seed. The amplitude and duration of the stimuli follow a uniform distribution between a lower limit (l_{lower}) and an upper limit (l_{upper}). Then, if $l_{lower} < 0$ and $l_{upper} > 0$, the EPSP rate (EPSP rate) can be estimated as:

$$EPSP_{rate} = \frac{|l_{upper}|}{|l_{upper} - l_{lower}|}$$

As for the IPSP rate ($IPSP_{rate}$), it can be estimated as follows:

$$IPSP_{rate} = \frac{|l_{lower}|}{|l_{lower} - l_{upper}|}$$

METHODOLOGY FOR ANALYZING BURST RESPONSES OF TRNN

From the above parameters and using a NEURON simulation environment [41, 42], it follows that an applied alternative methodology could allow for an approximation of the way the TRNn, or any other type of neuron, respond to changes in body temperature. It could determine the relationship between the burst mode response frequency (f) of the TRN neuronal model (TRNnm) and physiological temperature (T) with specific G_T values (figure 2A).

Table 1. Geometrical characteristics of the TRN model

Cell area	15115.5μm²
Soma's length	23819.8μm²
Soma's diameter	14.0754μm²
Soma 's area	1527.62μm²
N° segments (sections)	81
N° line segments (neuronal sector in straight line)	1444
N° distal dendrites	60
N° medial dendrites	13
N° proximal dendrites	7

Fuente: datos tabulados por los autores.
This geometrical model was obtained from reference [44]. The cell area using the procedure described in [52]

Table 2. Active and passive electrical conduction properties of the neuronal model

Property	Soma	Proximal Dendrites	Medial Dendrites	Distal Dendrites
G_{NaHH2} (S/cm^2)	0.1	-----	-----	-----
G_{KHH2} (S/cm^2)	0.08	-----	-----	-----
G_T(S/cm^2)	4.5x10^{-5}	4.5x10^{-5}	4.5x10^{-5}	[5.8,10]x10^{-5}
G_{pass}(S/cm^2)	5.0x10^{-5}	5.0x10^{-5}	5.0x10^{-5}	5.0x10^{-5}
E_{Na}(mV)	50	-----	-----	------
E_K(mV)	-100	-----	-----	------
E_T(mV)	120	120	120	120
E_{pass}(mV)	31.64	-82	-82	-82
R_a(Ω/cm)	260	260	260	260
C_m (μF/cm^2)	1	1	1	1
K_d (mM)	1x10^{-4}	1x10^{-4}	1x10^{-4}	1x10^{-4}

Fuente: datos tabulados por los autores.
This biophysical model was obtained from reference [44]. G_{NaHH2}: Maximum specific Sodium conductance; G_{KHH2}: Maximum specific Potassium conductance; G_T: Maximum specific low threshold calcium conductance (for the distal dendrites, this values varies in a range [5.8, 10] x10^{-4} S/cm^2); G_{pass}: Specific leak conductance; E_{Na}: Sodium equilibrium potential; E_K: Potassium equilibrium potential; E_T: Calcium equilibrium potential; E_{pass}: Leak equilibrium potential; R_a: Axoplasmic resistance; C_m: Specific membrane capacitance; K_d: Dissociation constant (assuming a Michaelis-Menten approximation for a simple model of ATPase calcium pump). The dashed line indicates the absence of the property.

Table 3. Formulas and constants using to model the variations of the intracellular concentration of Ca+2

General formula	$\frac{d[Ca^{+2}]_{in}}{dt} = \frac{d[Ca^{+2}]_{I_T}}{dt} - \frac{d[Ca^{+2}]_{pomp}}{dt} - \frac{d[Ca^{+2}]_{res}}{dt}$
I_T current	$\frac{d[Ca^{+2}]_{I_T}}{dt} = -\frac{10000\, I_T}{2Fd}$
Calcium pump	$\frac{d[Ca^{+2}]_{pomp}}{dt} = -\frac{K_T[Ca^{+2}]_{in}}{[Ca^{+2}]_{in} + K_d}$
Buffering	$\frac{d[Ca^{+2}]_{res}}{dt} = -\frac{[Ca^{+2}]_{in} - [Ca^{+2}]_{res}}{\tau_{aur}}$
Faraday constant	F = 96489C/mol
Depth of shell under the cell membrane	d = 0.1μm^2
Time constant of the pump	K_T= 1mM/s
Dissociation constant	K_d= 5x10^{-4}mM
Time constant	τ_{aur}= 700ms
The calcium resting level	$[Ca^{+2}]_{res}$

Fuente: datos tabulados por los autores.

Table 4. Formulas and constants used to model the activation processes of IT current

IT current	$I_T = \overline{g}_{Ca} m_{Ca}^2 h_{Ca}(V - E_{Ca})$
Activation variable	$\frac{dm_{Ca}}{dt} = -\frac{1}{\tau_{mCa}(V)}(m_{Ca} - m_{Ca\infty}(V))$
Inactivation variable	$\frac{dh_{Ca}}{dt} = -\frac{1}{\tau_{hCa}(V)}(h_{Ca} - h_{Ca\infty}(V))$
Steady-state activation function	$m_{Ca\infty}(V) = 1/[1 + \exp(-(V + 50)/7.4)]$
Steady-state inactivation function	$h_{Ca\infty}(V) = 1/[1 + \exp(-(V + 78)/5)]$
Activation time constant	$\tau_{mCa}(V) = (3 + 1/[a_{mCa} + b_{mCa}])/k_m$
a_{mCa}	$a_{mCa} = \exp((V + 25)/10$
b_{mCa}	$b_{mCa} = \exp(-(V + 100)/15$
Inactivation time constant	$\tau_{hCa}(V) = (85 + 1/[a_{hCa} + b_{hCa}])/k_h$
a_{hCa}	$a_{hCa} = \exp((V + 46)/4$
b_{hCa}	$b_{hCa} = \exp(-(V + 405)/50$
Temperature coefficient of activation	$k_m = 5^{\frac{T-24}{10}}$
Temperature coefficient of inactivation	$k_m = 3^{\frac{T-24}{10}}$
Equilibrium potential	$E_{Ca} = \frac{[1x10^3 R(T + 273.15)]}{2F} \ln(\frac{[Ca^{+2}]_{out}}{[Ca^{+2}]_{in}})$

Fuente: datos tabulados por los autores.

Table 5. Formulas and constants used to model the fast sodium channels

Sodium current	$I_{Na} = \overline{g}_{Na} m_{Na}^3 h_{Na}(V - E_{Na})$
Sodium activation variable	$\frac{dm_{Na}}{dt} = -\frac{1}{\tau_{mNa}(V)}(m_{Na} - m_{Na\infty}(V))$
Sodium inactivation variable	$\frac{dh_{Na}}{dt} = -\frac{1}{\tau_{hNa}(V)}(h_{Na} - h_{Na\infty}(V))$
Sodium steady-state activation function	$m_{Na\infty}(V) = a_{mNa}/(a_{mNa} + b_{mNa})$
Sodium steady-state inactivation function	$h_{Na\infty}(V) = a_{hNa}/(a_{hNa} + b_{hNa})$
a_{mNa}	$a_{mNa} = 0.32(13 - V_2)/[\exp((13 - V_2)/4) - 1]$
b_{mNa}	$b_{mNa} = 0.28(V_2 - 40)/[\exp((V_2 - 40)/5) - 1]$
a_{hNa}	$a_{hNa} = 0.128\exp((17 - V_2)/18)$
b_{hNa}	$b_{hNa} = 4/[1 + \exp((40 - V_2)/5)]$

V_2	$V_2 = V - V_{traub}$
V_{traub}	$V_{traub} = -63mV$
Sodium activation time constant	$\tau_{mNa}(V) = (1/[a_{mNa} + b_{mNa}])/k_{NaK}$
Sodium inactivation time constant	$\tau_{hNa}(V) = (1/[a_{hNa} + b_{hNa}])/k_{Na}$
Temperature coefficient of sodium	$k_{Na} = 3^{\frac{T-36}{10}}$
Channels sodium equilibrium potential	$E_{Na} = 50mV$

Fuente: datos tabulados por los autores.

Table 6. Formulas and constants used to model the fast potassium channels

Potassium current	$I_K = \overline{g}_K n_K^3 h_K (V - E_K)$
Potassium activation variable	$\frac{dn_K}{dt} = -\frac{1}{\tau_{mK}(V)}(n_K - n_{K\infty}(V))$
Potassium steady-state activation function	$n_{K\infty}(V) = a_{nK}/(a_{nK} + b_{nK})$
anK	$a_{nK} = 0.032(15 - V_2)/[\exp((15 - V_2)/5) - 1]$
bnK	$b_{nK} = 0.5\exp((10 - V_2)/40)$
ahK	$a_{hK} = 0.128\exp((17 - V_2)/18)$
bhK	$b_{hK} = 4/[1 + \exp((40 - V_2)/5)$
Potassium activation time constants	$\tau_{nK}(V) = (1/[a_{nK} + b_{nK}])/k_K$
Temperature coefficient of potassium channel	$k_K = 3^{\frac{T-36}{10}}$
Potassium equilibrium potential	$E_K = -90mV$

Fuente: datos tabulados por los autores.

RESULTS

The results of this work are focused, first, on the analysis of the relationships between f_{max} in burst mode and the corresponding temperatures (see Figure 2B). Second, the results are focused on f_{max} and the G_T at which it was obtained (see Figure 2C). Third, they are centered on the relationship between ΔT_h and the corresponding f_{max} values (see Figure 3A), and the relationship between ΔT_h and G_T (see Figure 3B). ΔT_h is a parameter proportional and representative of the temperature range at which TRNn can respond in burst mode (see Figure 3A).

Figure 2A shows the relationship between the burst mode response frequency (f) of the TRNnm and physiological temperature (T) for $G_T = 8$ S/cm^2, and for a temperature range in which burst discharges were observed. T_{h1} and T_{h2} are the temperatures at which the TRNnm can respond in burst mode with a frequency equal to half

the maximum frequency (i.e. $f = f_{max}/2$). $\Delta T_h = T_{h2} - T_{h1}$ is full width at half maximum. T_{fmax} is the temperature at which the TRNnm fires in burst mode at maximum frequency. It was found that for any G_T value in the range of [5,8,10] S/cm^2, the curve fitted to points (f,T) is always biased to the left (negative asymmetry) in a maximum temperature range [12,44]°C, and the fitted equations were degree 10 polynomials. All the parameters that generated the results of this work were based on the development of graphics similar to Figure 2A (f vs. T) and for different G_T values in the aforementioned range.

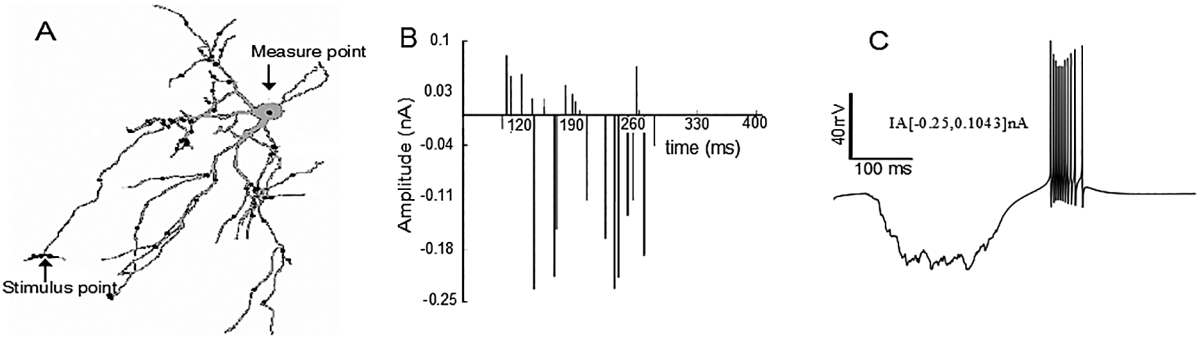

Figure 1. Burst simulation in the neuronal soma after trains of random stimuli were applied on the distal dendrites. Burst simulation in the neuronal soma after trains of random stimuli were applied on the distal dendrites. A) Note the measuring point (black arrow) on the soma and the stimuli points (gray dots) on the distal dendrites. B) The train of random current stimuli with negative and positive amplitudes. C) Burst neuronal response due to random stimuli in the amplitude range IA[-0.25, 0.1043] nA applied to the distal dendrites. Note that the burst in C has the same characteristics of the typical burst (reference burst) shown in [43, 15].

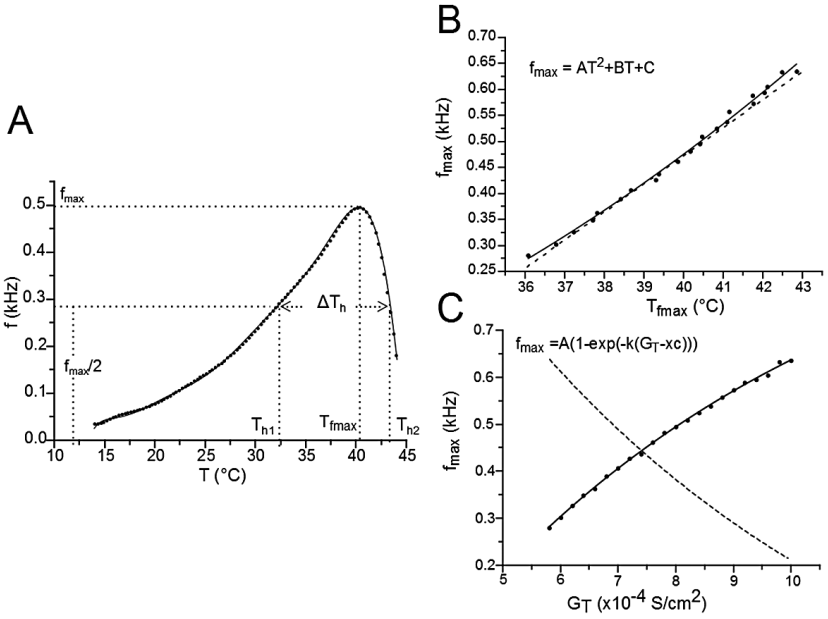

Figure 2. Frequency changes (f) during burst mode responses for different G_T values. A) The variation of f for $G_T = 8x10^{-4}$ S/cm^2 and for different temperatures was fitted to a polynomial equation. For

other values of G_T, the equation fitting was similar. T_{h1} and T_{h2} are the temperatures at which the TRNnm responds in burst mode with a frequency equal to half the maximum frequency ($f = f_{max}/2$). $\Delta_{Th} = T_{h2} - T_{h1}$. Tf_{max} is the temperature at which the TRNnm fires in burst mode at maximum frequency. For any value of G_T, this curve always shows a negative asymmetry. B) Relationships between f_{max} and T_{fmax}. The points (f_{max},T_{fmax}) on the solid line were fitted to a growth quadratic equation (Eq. 1). C) Nonlinear relation between f_{max} and G_T. The points (f_{max},G_T) on the solid line were fitted to a growth exponential equation. The dashed lines in B) and C) represent the first derivative of equations 1 and 2, respectively.

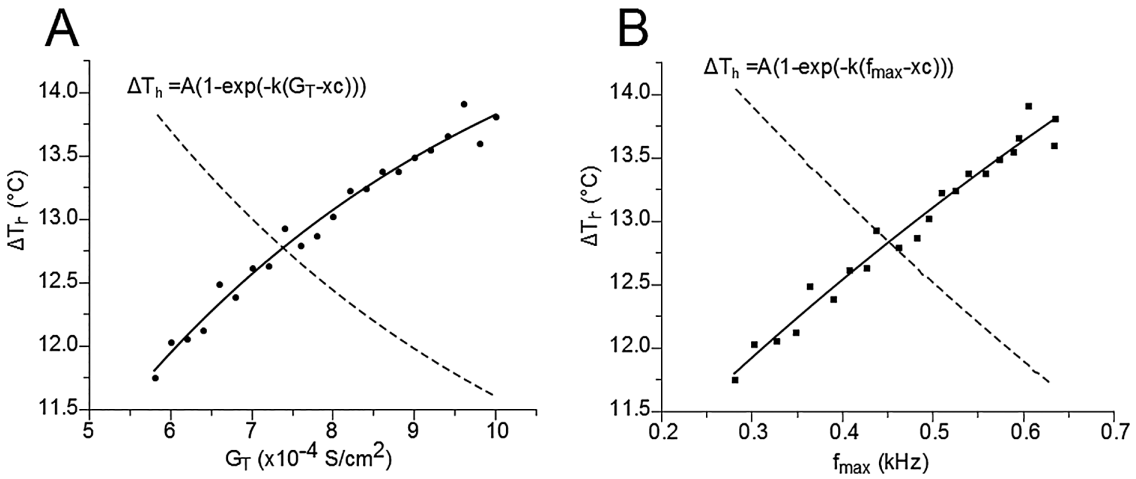

Figure 3. Relationship between the representative temperature range (ΔT_h) at which the TRNnm responds in burst mode, the maximum calcium conductance (G_T), and the maximum burst frequency (f_{max}). In both cases, A) and B), the points of the curves are fitted to an exponential growth equation.

The solid line in Figure 2B shows the relation between f_{max} and T_{fmax} and its points fitted to a growth quadratic equation (Eq. 1, with $R^2 = 0.99623$).

$$f_{max} = 0.0014225T_{max}^2 - 0.05702T_{max} + 0.48045 \quad (1)$$

The dashed line in Figure 2B represents the first derivative of equation 1 (see eq. 2). It shows that as temperature rises, the maximun burst mode firing frequency per unit temperature of the TRNnm increases in linear and growing form. Thus, for example, at T = 37°C, f_{max} increases by 1 kHz for each temperature increase of 1°C; and at T = 40°C, f_{max} increases by 1354 kHz for each temperature increase of 1°C. 2.485x10^{-3}Hz/°C/°C represents the slope of the line and shows the steady increase of dfmax/dT per unit temperature increase, i.e., df_{max}/dT increases by 2.485 x10^{-3}Hz/°C for each temperature increase of 1°C.

$$\frac{df_{max}}{dT} = 2.845x10^{-3}T_{max} - 0.057027 \quad (2)$$

The points (f_{max}, G_T) were also fitted to a growth curve, but in this case following an exponential relation (eq. 3, with $R^2 = 0.99901$), as shown by Figure 2C. 1.0529 kHz represents the maximum value that f_{max} can reach no matter how high the G_T is. In equation 3, it can be seen that this saturation value is obtained for very large values of G_T (if G_T approaches infinity). However, this TRNnm

can only respond with typical burst activity for the range of conductances [5.8, 10] S/cm^2.

$$f_{max} = 1.0529\ (1 - e^{-0.14701(G_T - 3.686)}) \quad (3)$$

The dashed line in Figure 2C corresponds to the first derivative of equation 3 (see eq. 4). It shows that as G_T increases, the maximum frequency changes observed in the TRNnm decrease exponentially, i.e., df_{max}/dG_T decreases if G_T increases, and tends to zero if G_T tends to infinity. For example, for $G_T = 6x10^{-4}$ S/cm^2, df_{max}/dG_T decreases by 0.11 kHz/($1x10^{-4}$ S/cm^2) for each unit increase ($1x10^{-4}$ S/cm^2) in maximum Ca^{+2} conductance. For $G_T = 8x10^{-4}$ S/cm^2, f_{max} decreases by 0.08 kHz/($1x10^{-4}$ S/cm^2) for each G_T increase of $1x10^{-4}$ S/cm^2.

$$\frac{df_{max}}{dG_T} = 3.8809e^{-0.14701(G_T - 3.686)} \quad (4)$$

Figure 3A shows the relationship between ΔT_h and G_T. The points (ΔT_h, G_T) were fitted to a growth exponential equation (eq. 5, with R^2= 0.97859). with the maximum value ΔT_h =15.321°C. This was expected since, despite being different equations, the same ΔT_h maximum values should be observed.

$$\Delta T_h = 15.321(1 - e^{-0.20333(G_T - 1.4469)}) \quad (5)$$

Figure 3B shows the relationship between ΔT_h and f_{max}. The points (ΔT_h, f_{max}) were fitted to a growth exponential equation (eq. 6, with R^2 = 0.96501). 15.321°C represents the maximum value that ΔT_h can reach independently of the f_{max} value.

This saturation value occurs if f_{max} tends to infinity.

$$\Delta T_h = 15.321(1 - e^{-2.3018(f_{max} - 0.34814)}) \quad (6)$$

From equations 5 and 6, it can be observed that f_{max} = 0.086 kHz and G_T = 6.37 S/cm^2 represent the values at which ΔT_h reaches a value equal to 63% of its maximum possible value (15.321°C), i.e. ΔT_h = 9.65°C.

DISCUSSION

The physiological temperature of mammals may vary depending on different normal or pathological causes [50]. However, the electrical response of the different types of neurons to normal and pathological temperature variations is not fully understood [51]. This study presents a novel methodological alternative based on computational simulations, which allows for predicting the way different types of neurons respond to changes in body temperature. The following parameters were defined for each frequency (f) versus temperature (T) graphic with specific G_T values: full width at half maximum (ΔT_h) as a measure of the temperature range at which a neuron responds in burst mode, f_{max}, and the temperature at which this frequency occurs (T_{fmax}). Next, based on the development of this same graph for different G_T values, graphics 2B, 2C, 3A and 3B were obtained.

The results of this study are a faithful approximation to reality due to four main reasons. First, the use of a morphology (neuronal geometry) obtained from a neuronal reconstruction (intact TRN cell with 80 compartments) that entails real dimensions. Second, the biophysics incorporated to the model allows reproducing different types of neuronal responses and their properties. Third, the applied stimulus takes into account the randomness of the amplitudes and durations of both inhibitory and excitatory stimuli originating in other TRNn and in collaterals of thalamocortical and corticothalamic neurons,

respectively. Fourth, consistent with previous experimental studies, this study found that the effects of temperature changes in T-type Ca^{+2} channels are nonlinear (see Figures 2, 3 and equations 1, 3, 5 and 6).

All results obtained in this work correspond to a specific TRNnm. Nonetheless, T- type Ca^{+2} channels cause the observed bursting activity. The following observations highlight some of the most relevant results of this study and their electrophysiological implications.

Figure 2B and Equation 1 show that for a constant conductance, increases in physiological temperature cause an increase in the maximum firing frequency and the effect is greater for higher temperature values. Although the quadratic growth model shown in figure 2B and equation 1 suggests that there is no f_{max} limit for any temperature increase, figure 2C and equation 3 show that for high G_T values, maximum firing frequency of the TRNnm always tends to an f_{max} limit. For the model used in this work, the limit tends to f_{max} = 1.0529 kHz

The results in Figure 2 show that the development of computational neuronal models incorporating reality-adjusted biophysics and geometry, can contribute to predicting the behavior of a neuron for different T-type calcium conductances and physiological temperatures. The curves fitted to Figures 2B and 2C (see equations 1 and 3, respectively) have determination coefficients very close to a unit (R^2=0.996), which shows the reliability of the model.

Figure 3A and equation 5 show that if TRNn display bursting activity with high f_{max} values, then they can display such responses through a wide range of temperatures. In addition, Figure 3B and equation 6 show that if bursting activity caused by T-type calcium conductances for high G_T values is observed in a neuron similar to TRNn, then it can exhibit this kind of response through a wide range of temperatures. Specifically, the proper functioning of T-type Ca^{+2} channels after broad physiological temperature variations (increase or decrease) depends on G_T. From Equations 5 and 6, it can also be inferred that if G_T = 6.37 S/cm^2 and bursting activity is observed at a maximum frequency of 0.086 kHz, then this neuron can exhibit the same type of activity through a range of temperatures ΔT_h > 9.65°C.

CONCLUSIONS

Based on a computational TRNnm that responds in burst mode due to the application of the same type of random stimulus (see Figure 1) at different points of the distal dendrites, it can be concluded that:

First, for constant G_T, the maximum firing frequency of TRNn varies proportionally and in quadratic relation to the temperature at which it occurs (see Equation 1). This equation shows that for the same specific T-type calcium conductance, increases in physiological temperature cause an increase in the maximum firing frequency and the effect is greater for increments in temperature values.

Second, the maximum frequency at which TRNn respond in burst mode varies proportionally and in exponential growth relation to the maximum Ca^{+2} conductance (see Equation 3). This equation shows that for increments in the values of G_T, the maximum firing frequency always tends to an f_{max} limit.

Third, ΔT_h is a representative value of the temperature range (ΔT) at which specific TRNn respond in burst mode, and its relation to the

maximum firing frequency in burst mode (ΔT_h vs. f_{max}) was fitted to an exponential growth (see Equation 6). This equation shows that if specific TRNn display bursting activity with f_{max} values, they can also display this type of behavior through a wide range of temperatures.

Finally, and similar to the above relationship (ΔT_h vs. f_{max}), ΔT_h vs. G_T was fitted to an exponential growth equation (see Equation 5). This equation shows that the proper functioning of T-type Ca^{+2} channels after broad physiological temperature variations depends on G_T.

Conflict of interest: none.

Financing: own resources.

REFERENCES

1. McCormick DA, Prince DA. Acetylcholine induces burst firing in thalamic reticular neurones by activating a potassium conductance. *Nature* 1986;319(6052): 402 - 405. doi:10.1038/319402a0
2. Muñoz F, Fuentealba P. Dynamics of action potential initiation in the gabaergic thalamic reticular nucleus in vivo. PLoS *ONE* 2012; 7(1): 30154 doi:10.1371/journal.pone.0030154.
3. Mukhametov LM, Rizzolatti G, Tradardi V. Spontaneous activity of neurones of nucleus reticularis thalamic in freely moving cats. *J Physiol* 1970; 210(3):651 - 667
4. Domich L, Oakson G, Steriade M. Thalamic burst patterns in the naturally sleeping cat: a comparison between cortically projecting and reticularis neurones. *J. Physiol* 1986;379:429-449
5. Tabares L, Lopez-Barneo J. Canales de calcio. *In Biofísica y Fisiología Celular,* pp. 311-333. Universidad de Sevilla, (1996). Google-Books-ID: jgVxyb2JlOgC
6. Yunker AMR, McEnery MW. Low-voltage-activated (t-type) calcium channels in review. *Journal of Bioenergetics and Biomembranes* 2003; 35(6): 533 – 575. doi:10.1023/B:JOBB.0000008024.77488.48.
7. Huguenard JR. Low-threshold calcium currents in central nervous system neurons. Annu. *Rev. Physiol.* 1996;58:29-348. doi:10.1146/annurev.ph.58.030196.001553
8. Perez-Reyes E. Molecular physiology of low-voltage-activated t-type calcium channels. *Physiol. Rev.* 2003; 83(1):117-161. doi:10.1152/physrev.00018.2002
9. Berridge MJ, Lipp P, Bootman MD. The versatility and universality of calcium signalling. *Nat Rev Mol Cell Biol* 2000;1(1): 11-21. doi:10.1038/35036035.
10. Crunelli V, Lightowler S, Pollard CE. A t-type ca2+ current underlies low-threshold ca+2 potentials in cells of the cat and rat lateral geniculate nucleus. *The Journal of Physiology* 1989;413(1): 543-561. doi:10.1113/jphysiol.1989.sp017668.
11. Destexhe A, Neubig M, Ulrich D, Huguenard J. Dendritic low-threshold calcium currents in thalamic relay cells. *J. Neurosci* 1998;. 18(10):3574-3588.
12. Konnerth A, Lux H. Proton-induced transformation of calcium channel in chick dorsal root ganglion cells. *The Journal of Physiology* 386 1987; 603-633. doi:10.1113/jphysiol.1987.sp016864.
13. Koustyuk Ya, Shuba M. Three types of calcium channels in the membrane of mouse sensory neurons. *European Journal of physiology* 1988; 411:661-669
14. Williams ME, et al. Structure and Functional Characterization of a Novel Human Low-Voltage Activated Calcium Channel. *Journal of neurochemistry* 1999; 72(2):791-799
15. Hernandez O, Hernandez L, Vera D, Santander A, Zurek E. Thalamic reticular cells firing modes and its dependency on the frequency and amplitude ranges of the current stimulus. *Med Biol Eng Comput* 2015; 53(1), 37-44. doi:10.1007/s11517-014-1209-z
16. Burns BD, Pritchard R. Contrast discrimination by neurons in the cats visual cerebral cortex. *J. Physiol* 1964; 175:445- 463

17. Cattaneo A, Maei L, Morrone C. Patterns in the discharge of simple and complex visual cortical cells. Proc. R. Soc. *Lond., B, Biol. Sci.* 1981; 212(1188):279 - 297
18. Segundo JP, Moore GP, Stensaas LJ, Bullock TH. Sensitivity of neurones in aplysia to temporal pattern of arriving impulses. *Journal of Experimental Biology* 1963; 40(4): 643-667
19. Eggermont JJ. Is there a neural code? *Neurosci Biobehav Rev* 22(2): 355-370
20. Lesica NA, Stanley GB. Encoding of natural scene movies by tonic and burst spikes in the lateral geniculate nucleus. *J. Neurosci.* 2004;24(47): 10731-10740 doi:10.1523/JNEUROSCI.3059-04.2004.
21. Lundstrom BN, Fairhall AL. Decoding stimulus variance from a distributional neural code of interspike intervals. *J. Neurosci.* 2006; 26(35):9030-9037. doi:10.1523/JNEUROSCI.0225-06.2006
22. Reinagel P, Godwin D, Sherman SM, Koch C. Encoding of visual information by LGN bursts. *J. Neurophysiol.* 1999;81(5):2558-2569
23. Crick F. Function of the thalamic reticular complex: the searchlight hypothesis. *Proc. Natl. Acad. Sci.* 1984; 81(14):4586-4590
24. Nicolelis MAL, Fanselow EE. Thalamocortical correction of thalamcortical optimization of tactile processing according to behavioral state. *Nat. Neurosci.* 2002; 5(6):517-523. doi:10.1038/nn0602-517
25. Iftinca M, McKay BE, Snutch TP, McRory JE, Turner RW, Zamponi GW. Temperature dependence of t-type calcium channel gating. *Neuroscience* 2006;142(4):1031-1042. doi:10.1016/j.neuroscience.2006.07.010
26. Weiss N, Black SAG, Bladen C, Chen L, Zamponi GW. Surface expression and function of cav3.2 t-type calcium channels are controlled by asparagine-linked glycosylation. *Pugers Arch - Eur J Physiol* 2013; 465(8):1159-1170. doi:10.1007/s00424-013-1259-3.
27. Umemiya M, Berger AJ. Single-channel properties of four calcium channel types in rat motoneurons. *J. Neurosci.* 1995;15(3 Pt 2):2218-2224
28. Monteil, A, Chemin J, Leuranguer V, Altier C, Mennessier G, Bourinet E, Lory P, Nargeot J. Specific properties of t-type calcium channels generated by the human α1 subunit. *J. Biol. Chem.* 2000; 275(22), 16530 – 16535. doi:10.1074/jbc.C000090200.
29. McRory JE, Santi CM, Hamming KSC, Mezeyova J, Sutton KG, Baillie DL, Stea A, Snutch TP. Molecular and functional characterization of a family of rat brain t-type calcium channels. *J. Biol. Chem.* 276(6), 3999 - 4011 (2001). doi:10.1074/jbc.M008215200.
30. Plonsey R, Barr RC. Action potentials. In: Bioelectricity. USA: *Springer,* 2007. 3ed pp. 97-153. Doi: 10.1007/978-0-387-48865-3 5
31. Hernández O, Hernández L. Relationship between hodgkin and huxley style sodium and potassium conductances and their effect on the propagation of action potentials at 40°C. *Revista Salud Uninorte* 2011; 27(2): 223-235
32. Fitzhugh R. Theoretical effect of temperature on threshold in the hodgkin-huxley nerve model. *J Gen Physiol* 1966; 49(5):989-1005
33. Rattay F, Aberham M. Modeling axon membranes for functional electrical stimulation. *IEEE Trans Biomed Eng* 1993; 40(12):1201-1209 doi:10.1109/10.250575
34. Narahashi T, Tsunoo A, Yoshii M. Characterization of two types of calcium channels in mouse neuroblastoma cells. *J. Physiol.* (Lond.) 383, 231-249 (1987)
35. Rosen AD. Temperature modulation of calcium channel function in GH3 cells. Am. *J. Physiol.* 1996; 271(3 Pt 1):863-868
36. Carnevale NT, Hines ML. The Neuron Book
37. Gewaltig MO, Diesmann M. Nest (neural simulation tool). *Scholarpedia* 2007; 2(4): 1430 doi:10.4249/scholarpedia.1430.
38. (38) Hines M, Carnevale NT. Computer Simulation Methods for Neurons.1994.
39. The Book of GENESIS: Exploring Realistic Neural Models with the GEneral NEural SImulations System. 1994: Springer, Santa Clara, Calif.
40. Bower JM, Cornelis H, Beeman D. Genesis, the general neural simulation system.

Encyclopedia of Computational Neuroscience 2015; 1287-1293. Doi: 10.1007/978-1-4614-6675-8 255

41. Hines ML, Carnevale NT. The neuron simulation environment. *Neural Comput* 1997; 9(6):1179-1209
42. Hines ML. Neuron - a program for simulation of nerve equations. In: Eeckman, F.H. (ed.) Neural Systems: Analysis and Modeling, pp. 127 - 136. *Springer*, (1993). DOI: 10.1007/978-1-4615-3560-7_11
43. Destexhe A, Contreras D, Steriade M, Sejnowski TJ, Huguenard JR. In vivo, in vitro, and computational analysis of dendritic calcium currents in thalamic reticular neurons. *J. Neurosci.* 16(1) 1996; 169-185.
44. Destexhe et al. ModelDB Thalamic reticular neurons: the role of Ca currents. Available in: https://senselab.med.yale.edu/modeldb/showModel.cshtml?model=17663
45. Pinault D, Deschenes M. Anatomical evidence for a mechanism of lateral inhibition in the rat thalamus. *Eur. J. Neurosci.* 1998; 10(11):3462-3469
46. Scheibel ME, Scheibel AB. Terminal axonal patterns in cat spinal cord. I. The lateral corticospinal tract. *Brain Res.* 1966; 2(4):333-350
47. Kim U, Sanchez-Vives MV, McCormick DA. Functional dynamics of gabaergic inhibition in the thalamus. *Science* 1997; 278(5335):130-134 doi:10.1126/science.278.5335.130.
48. (48) Xu NI. Ye CQ, Poo MM, Zhang XH. Coincidence detection of synaptic inputs is facilitated at the distal dendrites after long-term potentiation induction. *The Journal of Neuroscience* 2006; 26(11):3002-3009
49. (49) Hausser M, Spruston N. Stuart GJ. Diversity and dynamics of dendritic signaling 2000; 290(5492): 739-744
50. Hall JE. Body temperature regulation and fever, 13th edn., pp. 909-922 (2016). Chap. 74
51. Kushmerick C, Renden R, Gersdorff H. Physiological Temperatures Reduce the Rate of Vesicle Pool Depletion and Short-Term Depression via an Acceleration of Vesicle Recruitment. *The Journal of Neuroscience* 2006;26(5): 1366-1377 doi:10.1523/JNEUROSCI.3889-05.2006.
52. Hernández O, Jabba D, Muñoz F. Data exporter: A complementary tool to export data simulation from neuron. *Salud Uninorte* 2013;29(2): 288- 297.